1985

Study of Mo, Au, and Ni Implanted Molybdenum Laser Mirrors By Spectroscopic Ellipsometry

Paul G. Snyder
University of Nebraska-Lincoln

George H. Bu-Abbud
University of Nebraska-Lincoln

Jae Oh
University of Nebraska-Lincoln

John A. Woollam
University of Nebraska-Lincoln, jwoollam1@unl.edu

David Poker
Oak Ridge National Laboratory

See next page for additional authors

Manuscript Received
12-22-86

Study of Mo, Au, and Ni Implanted Molybdenum Laser Mirrors By Spectroscopic Ellipsometry*

Paul G. Snyder, George H. Bu-Abbud,+ Jae Oh, and John A. Woollam

University of Nebraska, Lincoln, NE 68588-0511

David Poker

Oak Ridge National Laboratory, Oak Ridge, TN 37830

D. E. Aspnes

Bell Communications Research, Inc., Murray Hill, NJ 07974

David Ingram and Peter Pronko

Universal Energy Systems, Dayton, OH 45432

The implantation of 150 kev molybdenum ions into polished molybdenum laser mirrors is found to increase the complex dielectric constant in the visible spectrum. Analysis using the Bruggeman effective medium approximation demonstrates that the increase is due to surface smoothing, and that the surface is made nearly atomically smooth by a fluence of 5 x $10^{15}/cm^2$. Implantation of Au at 1Mev caused considerable microscopic roughening, as well as a change in the bulk optical properties. 3 MeV Ni ion implantation caused only a slight surface roughening. A thin dielectric film (probably a hydrocarbon) is found to condense in a laboratory atmosphere, reducing the reflectivity, and is removable by rinsing with methanol and distilled water.

Key Words: Molybdenum laser mirrors; spectroscopic ellipsometry; ion implantation; surface smoothing.

1. Introduction

Molybdenum is of interest as a laser mirror material because it possesses desirable thermal properties [1]. Various techniques for producing very smooth, highly reflecting surfaces have been investigated, including mechanical and electrochemical polishing [1,2], chemical vapor deposition [3], and ion implantation[4,5]. The optical properties of Mo prepared by bulk and thin film techniques have been studied using several methods [6], among them ellipsometry [5,6,7], reflectance [6,8], and reflectance and transmittance [9] measurements. Roughness and microstructure of molybdenum surfaces have been studied by Nomarski imaging, profilometry, and total integrated scattering [1,2,5,10,11]. In this paper we present the results of single and multiple angle of incidence spectroscopic ellipsometric measurements in the visible to near ultraviolet on polished Mo mirrors which have been implanted with 150 keV Mo, 1 MeV Au, or 3 MeV Ni ions. We describe the effect of implantation on the Mo mirror optical properties for a wide range of fluences.

2. Samples and Experiment

Three commercially prepared vacuum arc cast [1] molybdenum mirrors, about 4 cm in diameter, were mechanically polished with alumina to a final grit size of 0.3 micron. Chemical analysis of

*Research supported in part by the U.S. Department of Energy under contract DE-AC05-84OR21400 at ORNL, NSF/SBIR Grant PHY-8318798, and the College of Engineering, UNL.
+Present Address: Reliance Comm/TEC, Advanced Development Lab, Richardson, TX 75081

the starting molybdenum surfaces showed there to be less than the following percentages of impurities: 0.005 carbon, 0.008 iron, 0.002 nickel, 0.008 silicon, 0.0015 oxygen, 0.0005 hydrogen, 0.002 nitrogen. Six 1 x 3 cm^2 regions on each mirror were implanted at room temperature with fluences from 1 x 10^{14} to 5 x $10^{15}cm^{-2}$, the first mirror with 150 keV Mo ions, the second with 1MeV Au ions, and the third with 3 MeV Ni ions. All implantations were made at room temperature, because it was found in previous work that heating the substrate during implantation caused an increase in the surface roughness [5]. The Mo implantation was performed at Oak Ridge National Laboratories on a 200 keV Varian "Extrion", and Au and Ni were implanted on a 6 MeV General Ionex "Tandetron" at Universal Energy Systems. Reflection of a helium-neon laser beam from all of the implanted surfaces was specular, with no distortion of the beam.

Two automatic rotating analyzer ellipsometers were used. One, at Bell Communications Research Inc., had an angle of incidence ϕ fixed at 67.08° and a photon energy scanning range of 1.5 to 6 eV [12]. It was used to measure the ellipsometric parameters $\tan\psi$ and $\cos\Delta$ for the various regions on the Mo implanted mirror. Contamination effects were minimized by optically prealigning the mirror in a windowless cell, cleaning its surface by rinsing in sequence with distilled water, methanol, and distilled water, and then maintaining its surface in dry filtered N_2 during measurement.

The other ellipsometer, at the University of Nebraska-Lincoln, was similar in design to the first, but had a variable angle of incidence [5]. It was used to collect all of the data for the Au and Ni implanted mirrors, and some data for the Mo implanted mirror. Measurements were made at angles of incidence from 71° to 79°, and at photon energies from 1.8 to 3.8 eV. The Au implanted mirror was prealigned and rinsed as described above, then blown dry with high purity Argon. Data were obtained within several minutes of rinsing. The Ni implanted mirror was not rinsed at all before measuring. When the rinsing procedure was performed on the Mo implanted mirror, the two ellipsometers produced almost identical pseudodielectric function data for this carefully cleaned sample in the overlapping energy range, as shown in figure 1, despite the fact that data were obtained at different angles of incidence. This demonstrates that data from the Bellcore and UNL ellipsometers agree with each other to better than one percent when proper surface preparation procedures are followed. Multiple angle of incidence data provided additional information about the surface and bulk optical properties, as described below.

3. Mo Implanted Mirror

The pseudodielectric function is the effective, or apparent, dielectric response calculated from the measured ψ and Δ values at any given photon energy and angle of incidence, ϕ, by assuming a two-phase (smooth substrate-ambient) model [13]:

$$\langle\varepsilon\rangle = \langle\varepsilon_1\rangle - j\langle\varepsilon_2\rangle = \sin^2\phi\left[1+\left(\frac{1-\tan\psi e^{j\Delta}}{1+\tan\psi e^{j\Delta}}\right)^2\tan^2\phi\right] \qquad (1)$$

Pseudodielectric functions $\langle\varepsilon\rangle$ for the various regions on the Mo implanted mirror surfaces, for fluences from 1 x $10^{14}cm^{-2}$ to 5 x $10^{15}cm^{-2}$, are shown in figure 2. There is little apparent change in $\langle\varepsilon\rangle$ as the fluence is increased from 1 x $10^{14}cm^{-2}$ to 1 x $10^{15}cm^{-2}$, but at 2 x $10^{15}cm^{-2}$ both $\langle\varepsilon_1\rangle$ and $\langle\varepsilon_2\rangle$ are significantly changed over the entire spectrum. Increasing the fluence to 5 x$10^{15}cm^{-2}$ causes a slight further increase in $\langle\varepsilon_2\rangle$.

The changes in $\langle\varepsilon\rangle$ described above could be due to thickness changes of a dielectric overlayer, or to changes in the substrate microstructure (as in a loss of crystallinity), or to changes in the surface microscopic roughness. While we have observed thin films to physisorb onto Mo surfaces, such films are completely removable by the rinsing procedure described above. A very thin passivating layer of natural oxide [14] is also known to grow on Mo. In a previous study [5] electron spectroscopy for chemical analysis (ESCA) measurements detected less than 10 Å of MoO_2 on Mo surfaces. No attempt was made to remove the oxides from our samples, because the necessary reactants would also have attacked the metal and roughened the surface. Even a very thin (monolayer) oxide will have a small effect on the $\langle\varepsilon\rangle$ data, but this effect should be essentially the same for all samples. Thus physisorbed films or natural oxides cannot explain the differences in figure 2. Secondly, there is no broadening or shifting of the $\langle\varepsilon\rangle$ spectral features with increasing fluence, which indicates that there is no implantation-induced change in crystallinity or grain size near the surface [15]. We conclude that the changes in $\langle\varepsilon\rangle$ with implantation fluence are due to changes in microscopic roughness.

We call attention to the fact that we are using the terminology "microstructure" in the standard materials science convention, that is, to refer to inhomogeneities on a length scale of

the order of 1 to 100 nm [16]. In the optics literature, "microstructure" is commonly used to refer to what we would call macrostructural inhomogeneities, with length scales greater than 1000 nm, i.e., to inhomogeneities that can be resolved with an optical microscope (see, e.g., ref. 1). The distinction is important because quite different physical properties are involved: microstructure determines the dielectric discontinuity at the material-ambient interface, i.e., the reflectance properties or light loss from transmission into the substrate material, whereas macrostructure determines light loss from scattering. Ellipsometric data are essentially unaffected by macrostructure, while scattering data are essentially unaffected by microstructure.

The increase in magnitude of $\langle\varepsilon_2\rangle$ with increasing fluence indicates microscopic smoothing of the surface by Mo ion implantation. To verify this and to quantify the changes in microscopic roughness, a single-parameter model was fit to the measured (ψ,Δ) data using the Marquardt minimization algorithm [17,18]. The three phases of the model were the molybdenum substrate, a "roughness" layer consisting of equal volume fractions of Mo and voids (absence of any material), and the air ambient. The size of the void regions is assumed to be much less than the wavelength of light. The Bruggeman effective medium approximation [19] (EMA) was used to model the effective dielectric response of the roughness layer, and the layer thickness was the model parameter.

The reference ε spectrum for Mo was taken to be the $\langle\varepsilon\rangle$ spectrum for the Mo implanted region with a fluence of $5 \times 10^{15}\text{cm}^{-2}$, which is seen in figure 2 to have the highest values of $\langle\varepsilon_2\rangle$. This implies that the $5 \times 10^{15}\text{cm}^{-2}$ region comes closest to realizing the sharp interface between bulk and ambient that is assumed with the two-phase model.

The roughness layer thicknesses obtained in the analysis are given in table I. The sharp drop in thickness above $1 \times 10^{15}\text{cm}^{-2}$ correlates with the change in $\langle\varepsilon\rangle$ seen in figure 2. In addition, the calculations show that Mo ion implantation at fluences higher than $2 \times 10^{15}\text{cm}^{-2}$ does not significantly further decrease the surface roughness. These results are similar to those described in reference 5, in which the microscopic surface roughness of mechanically polished samples of molybdenum rolled sheet stock decreased when they were implanted at room temperature with 150 keV Mo ions at a fluence of $2 \times 10^{15}\text{cm}^{-2}$, but did not decrease further when higher fluences were used.

A two phase (substrate, ambient) model was also investigated, in which the substrate was an effective medium containing voids, and the void fraction was the single variable parameter. As before, the $\langle\varepsilon\rangle$ from the $5 \times 10^{15}\text{cm}^{-2}$ fluence region was used as the substrate ε. This model, which excludes the possibility of surface roughness, produced a poor fit to the data. Furthermore, when the two models were combined to allow both substrate voids and surface roughness to be treated together, the calculated substrate void fraction converged to zero in all cases. This further indicates that the changes in $\langle\varepsilon\rangle$ with fluence are due to changes in the surface rather than in the bulk microstructure.

4. Film Growth on Mirrors

When measurements were made with the sample surfaces in air or in unfiltered nitrogen from a high pressure gas cylinder, the ellipsometric data revealed the presence of a film growing on Mo surfaces. A small (<1%) decrease in $\langle\varepsilon_2\rangle$ due to the growing film was often detectable within a few minutes after rinsing, and a film several days old lowered both $\langle\varepsilon_2\rangle$ and $\langle\varepsilon_1\rangle$ by almost 20 percent as shown in figure 3. Complete film removal by the distilled H_2O-methanol-distilled H_2O rinse was confirmed by analysis of data taken immediately after rinsing. The film was not an oxide, which would not be removed by the simple rinse procedure. The film is probably due to hydrocarbon contaminants from the nitrogen cylinder and/or in the laboratory air.

It was also inadvertantly discovered that the film was not easily removed after the mirror had been left exposed to air in the lab for several months. This film was only slightly reduced in thickness by soaking for several hours in acetone and then rinsing with methanol and distilled H_2O. In contrast, the film on another polished Mo mirror which was kept in a desiccator jar over the same period of time was easily removed by rinsing. We suggest that the unremovable films are the result of catalytic decomposition of hydrocarbons on the Mo (or Mo-oxide) surface to form polymeric compounds, a process known to lead to contact failure in mechanical relays with transition metal contacts [20].

5. Au Implanted Mirror

The pseudodielectric functions of the Au implanted molybdenum mirror are shown in figure 4. These $\langle\varepsilon\rangle$ spectra were derived from multiple angle of incidence measurements of $\tan\psi$ and $\cos\Delta$. At

each photon energy measurements were made at two angles of incidence near the principle angle. Each $\langle\varepsilon\rangle$ spectrum of figure 4 (and also the UNL spectrum in fig. 1) is the average of the two spectra obtained by applying eq. 1 at each angle of incidence. The $\langle\varepsilon\rangle$ spectra of the lowest fluence region are almost identical to those of the unimplanted region, and to those of the lowest fluence region on the Mo implanted mirror. Therefore Au or Mo implantation at a fluence of 1 x $10^{14}cm^{-2}$ or less has practically no effect on the polished mirrors. Au ion fluences above $5x10^{14}cm^{-2}$ caused a monotonic lowering of $\langle\varepsilon_2\rangle$, and also caused the structure in both $\langle\varepsilon_2\rangle$ and $\langle\varepsilon_1\rangle$ to be washed out. As discussed in the preceeding section the former effect is due to microscopic surface roughening, while the latter is due to changes in the bulk dielectric function of the mirror material near the surface.

In addition to calculating the pseudodielectric functions, we used the multiple angle of incidence ellipsometry data to simultaneously solve for the wavelength dependent Mo optical constants, and the thicknesses and void fractions of the surface roughness layers. This was possible because the system configuration was overdetermined, there being four data points (ψ and Δ at two angles of incidence) at each wavelength, and only two unknowns (ε_1 and ε_2) plus the wavelength independent roughness layer thickness and void fraction. Thus by using multiple angle of incidence, multiple wavelength data, we were able to eliminate the effect of surface roughness and to calculate the "true" dielectric function of the substrate material. It was assumed that the optical constants of the molybdenum metal in the substrate are identical to those of the Mo in the roughness layer. The optical constants (ε_1,ε_2) were allowed to vary, as well as the roughness layer thickness and void fraction, to obtain the best fit to the data. The Bruggeman EMA was again used to model the surface roughness layer. The thickness and void fraction solutions were 12Å and 0.5, respectively. In figure 5 the calculated substrate dielectric function of the $1x10^{14}cm^{-2}$ region is compared directly to the pseudodielectric function of the same region, and also to the pseudodielectric function of the $5x10^{15}cm^{-2}$ region on the Mo implanted mirror. If the 5 x $10^{15}cm^{-2}$ Mo implantation actually yields a nearly atomically smooth surface, and if the cleaning procedure really removes all surface overlayers, then the "substrate" and Mo implanted spectra should agree. Figure 5 shows that this is indeed the case. Thus the validity of the above assumptions is demonstrated.

Model "substrate" solutions for the higher fluence regions are shown in figure 6, and the corresponding thicknesses and void fractions of the roughness layers are given in table II. As with the Mo implanted mirror, the primary effect of roughness is to lower $\langle\varepsilon_2\rangle$. Note that even after correcting for surface roughness, the spectral features become broadened with increasing fluence. In addition, the ε_1 is shifted to more negative values. Both indicate a disruption of the electronic structure of the Mo grains, that is, amorphization of the near-surface material. However, electron microscopy analyses on similar samples have shown that there is little or no change in grain size in Mo-implanted Mo surfaces [21]. A more likely reason for the change in spectral structure is the formation of dense dislocation loops near the surface. In Rutherford backscattering measurements less than 0.1% Au was detected near the mirror surface, therefore the "washing out" of spectral features is not due to alloying. These points are discussed in more detail below.

6. Ni Implanted Mirror

The pseudodielectric functions of the Ni implanted surfaces are shown in figure 7. The mirror was not rinsed before measurements, and thus was covered by a thin dielectric film similar to that described above. The effect of the film is similar to that of roughness, namely, it lowers $\langle\varepsilon\rangle$ (see fig. 3). However, because the optical constants of the film are different from those of Mo and from air, the thin dielectric film and roughness can be distinguished. Using the dielectric function of smooth Mo obtained in the previous section, we determined the thickness and dielectric function of the dielectric film and the thickness of the roughness layer as a function of fluence. A four-phase model was used, consisting of: a Mo substrate, a roughness layer (containing equal volumes of Mo and hydrocarbon material and modeled in the EMA), the hydrocarbon film, and the air ambient. The roughness corrected dielectric function in figure 5 was used to represent Mo in the model. The thickness of the roughness layer, as well as the thickness and dielectric function of the hydrocarbon films, were variables in the model. The hydrocarbon index of refraction was found to be 2.58 ± 0.1 over the entire photon energy range, and the results for the thicknesses are shown in table III. From the analysis we find that the Mo surface roughness decreases monotonically with increasing fluence to 1 x $10^{15}cm^{-2}$, at which point the trend reverses. In addition, a slight lowering and loss of optical structure was found for the Mo dielectric function at the highest fluence, indicating some disordering of the bulk crystalline structure near the surface. It is noteworthy that the initial smoothing trend with increasing fluence was not evident from the pseudodielectric functions. In contrast, for the Mo implanted mirror which had no film, the surface smoothing trend was observable in the pseudodielectric

function data of figure 2 as well as in the results of the analysis. Thus the effect of surface smoothing on $\langle\varepsilon\rangle$ is masked by the presence of the film. The increase in hydrocarbon film thickness with fluence seen in table III is probably an artifact resulting from the time span of several days over which the mirror was exposed to air while measurements were made.

7. Discussion

The dielectric function data show that 150 keV Mo implantation improves the surface microstructure of the Mo mirrors, while 3 MeV Ni initially improves it, and 1 MeV Au or further Ni implantation degrades it. The fact that both improvement and degradation are seen for the same target material provides an opportunity to gain information on the mechanisms involved.

To proceed further we need the implantation parameters for each of the three systems. These are given in table IV. The values of the ranges $\bar{x}$ and straggle lengths $\overline{\Delta x}$, and the deposited energies in the near-surface region for both electronic and nuclear loss mechanisms were calculated with the TRIM simulation code [22] using the nominal implantation energies and standard bulk density data for Ni, Mo, and Au. TRIM uses a linear binary collision approximation and assumes that the energy lost by a moving ion may be separated into electronic energy loss and nuclear energy loss. The former is rapidly dissipated in metals by plasmons and causes no permanent damage.

Nuclear energy loss may result in permanent damage if the kinetic energy transferred to a lattice atom in a collision exceeds a threshold value. For metals a reasonable value is 25 eV but it is strongly dependent (within a factor of two) on the direction of displacement within the crystal lattice and the elemental nature of the target. Not all atoms which are displaced from a lattice site to an interstitial position during the adiabatic phase of each ion cascade (<100 ps) remain displaced; some return to their original site as the lattice relaxes. The remaining interstitials will diffuse away until they are trapped by another vacancy, dislocation, or grain boundary (including the boundary at the vacuum surface), if the temperature of the lattice is high enough. The preferred trapping locations for these diffusing interstitials at the surface will be those which will reduce the free energy of the surface, i.e., jogs, steps, etc. The surface should be smoothed on a microscopic scale by interstitials diffusing to the surface if no additional roughening takes place because of some other property of the bombardment.

Because the optical data are only sensitive to the material properties of the first 20 nm (approximately) of the solid, it is important to examine the spatial properties of the ion cascades generated by the three ion species in molybdenum. The range parameters in table IV indicate that at the highest doses employed, the nickel content of the surface will be less than 1 ppm, and the gold content about 200 ppm. Although there are no data in the literature on the effect of small amounts of these impurities on the optical properties of molybdenum, one may assume that the levels of gold or nickel present in the molybdenum mirrors should have a negligible effect on the reflectance. Therefore the broadening seen in the bulk optical structure is not likely to be due to alloying effects.

Another effect which may cause broadening of $\langle\varepsilon\rangle$ spectra involves a change in grain size [15]. In a previous study [21], transmission electron microscopy was used to determine the grain size in molybdenum samples which had been polished mechanically, ending with a 1 μm diamond paste polish. No difference was found between unirradiated samples and samples irradiated with 150 keV molybdenum ions to a dose of $1\times10^{16}\,cm^{-2}$ at room temperature or 500^{o} C. The mean grain size was 250 nm with some evidence of plastic deformation due to the polishing. Thus a change in grain size is also not likely to be the cause of the spectral broadening. The broadening may be due to the formation of dense dislocation loops near the surface, caused by the collapse of small voids generated during the ion cascade.

Sputtering, or the loss of target atoms from the first one or two atomic layers which receive sufficient energy during the ion cascade to overcome the surface barrier energy, can in principle roughen an originally flat surface [23]. The ion cascade and hence the sputtering, which ensues when the cascade intersects the surface, is a localized event and results in material loss in the form of microscopic pits if the cascade is sufficiently dense [24]. This roughening process can compete with the smoothing process described above.

If the depth at which the majority of interstitials are created is much greater than the mean free path between trapping sites then the flux of interstials at the surface will be much less per incident ion for an ion which on average deposits its energy further below the surface than for an ion which on average deposits its energy nearer the surface. Thus the ion penetration depth will influence both the smoothing and roughening processes.

As an additional complicating effect, the sputtering rate can be greatly enhanced if the energy density of the ion cascades cannot be described by the "linear binary collision approximation". This can happen if the majority of atoms enveloped in each cascade are in motion and the cascade becomes nonlinear. This situation is referred to as an "energy spike".

For the ion target combinations examined here it is reasonable that the 150 keV molybdenum ions produce cascades which are "dilute" or "linear", and are sufficiently near the surface for the diffusing interstitials to smooth the surface faster than sputtering can roughen it. For 1 MeV gold the sputter rate is much larger than that for 150 keV molybdenum, which we speculate to be due to spike effects too large to be offset by the production of interstitials near the surface since the gold ion energy density is about twice that of the molybdenum ions. We postulate that the 3 MeV nickel ions in Mo produce deep diffuse cascades which generate interstitials which are trapped before reaching the surface. The sputtering that is generated causes the surface to roughen at a low rate compared to that of gold, and the sputtering rate for Mo is much lower than for both Au and Ni implants.

Thus the experimental data for Mo, Au, and Ni implants into Mo can be explained in terms of the ion energetics and competing smoothing and roughening processes.

8. Conclusion

The effects of ion implantation on the optical properties of highly polished molybdenum mirrors were determined using single and multiple angle of incidence spectroscopic ellipsometry. These measurements allowed us to obtain the bulk dielectric function of Mo from 1.5 to 6.0 eV as well as the thicknesses of surface roughness layers. The smoothest surfaces were obtained by implanting 150 keV Mo ions at a fluence of $5 \times 10^{15} cm^{-2}$, which produced a microscopically smooth surface. In contrast to reflectance measurements, the ellipsometric measurements are found to be very sensitive to microscopic roughness. A thin dielectric overlayer (probably a hydrocarbon) condensed on mirror surfaces exposed to air, considerably lowering the apparent dielectric function and also reducing the reflectance.

9. References

[1] J.M. Bennett, S.M. Wong and G. Krauss, Appl. Opt. 19, 3562 (1980).

[2] J.M. Bennett, P.C. Archibald, J.P. Rohr and A. Klugman, Appl. Opt. 22, 4048 (1983).

[3] G.E. Carver, Thin Solid Films 63, 169 (1979).

[4] R.A. Hoffman and W.J. Lange, "Ion Polishing of Optical Surfaces", Final Report to Air Force Weapons Laboratory from Westinghouse Research Laboratories AFWL-TR-76-155, September 1976.

[5] G.H. Bu-Abbud, D.L. Mathine, P.G. Snyder, J.A. Woollam, D. Poker, J.M. Bennett, D. Ingram and P.P. Pronko, J. Appl. Phys. 59, 257, (1986).

[6] J.H. Weaver, C. Krafka, D.W. Lynch and E.E. Koch, in Physics Data: Optical Properties of Metals I (Fachinformationszentrum Energie, Physik, Mathematik GmbH, Karlsruhe, 1981), p. 139.

[7] M.M. Kirillova, L.V. Nomerovannoya and M.M. Noskov, Sov. Phys. JETP 33, 1210 (1971).

[8] B.W. Veal and A.P. Paulikas, Phys. Rev. B10, 1280 (1974).

[9] J.E. Nestell, Jr. and R.W. Christy, Phys. Rev. B21, 3173 (1980).

[10] J.M. Bennett and J.H. Dancy, Appl. Opt. 20, 1785 (1981).

[11] J.M. Bennet, Opt. Eng. 24, 380 (1985).

[12] D.E. Aspnes and A.A. Studna, Appl. Opt. 14, 22 (1975).

[13] R.M.A. Azzam and N.M. Bashara, Ellipsometry and Polarized Light, North Holland Publishing Co., Amsterdam 1977.

[14] E. Deltombe, N. deZoubov, and M. Pourbaix, in Atlas of Electrochemical Equilibria in Aqueous Solutions, ed. by M. Pourbaix (National Association of Corrosion Engineers, Houston, 1974), p. 272.

[15] U. Kreibig, J. Phys. F4, 999 (1974).

[16] D.E. Aspnes, J.B. Theeten and F. Hottier, Phys. Rev. B20, 3292 (1979).

[17] D.W. Marquardt, J. Soc. Indus. Appl. Math. 11, 431 (1963).

[18] G.H. Bu-Abbud, N.M. Bashara, and J.A. Woollam, Thin Solid Films 138, 27 (1986).

[19] D.A.G. Bruggeman, Ann. Phys. 24, 636 (1935).

[20] H.W. Hermance and T.F. Egan, Bell System Tech. J. 37, 739 (1958).

[21] P. Pronko and D. Ingram, Phase 1 Report, "Ion beam processing for laser mirrors," NSF Award #PHY8260333, 1983.

[22] J. P. Biersack, J. Nucl. Instrum. Meth. 174, 257 (1980).

[23] J.E. Westmoreland and P. Sigmund, Radiation Effects **6**, 187 (1971).

[24] W. Jager and K.L. Merkle, 9th International Congress on Electron Microscopy, Vol. 1, p. 378 (1978).

Table 1. Mo Implanted Mo.

Fluence	Roughness Layer
$1 \times 10^{14} cm^{-2}$	13Å ± 1Å
$2 \times 10^{14} cm^{-2}$	13.5Å ± 1Å
$5 \times 10^{14} cm^{-2}$	16Å ± 1Å
$1 \times 10^{15} cm^{-2}$	14Å ± 1Å
$2 \times 10^{15} cm^{-2}$	0.5Å ± 0.5Å

Table 2. Au Implanted Mo.

Fluence	Roughness Layer	Void Fraction
$1 \times 10^{14} cm^{-2}$	12Å ± 1Å	0.5
$1 \times 10^{15} cm^{-2}$	22Å ± 3Å	0.43
$2 \times 10^{15} cm^{-2}$	62Å ± 10Å	0.39
$5 \times 10^{15} cm^{-2}$	130Å ± 20Å	0.6

Table 3. Ni Implanted Mo.

Fluence	Roughness Layer	Film Thickness
$2 \times 10^{14} cm^{-2}$	9Å ± 2Å	23Å ± 2Å
$5 \times 10^{14} cm^{-2}$	7Å ± 2Å	23Å ± 2Å
$1 \times 10^{15} cm^{-2}$	5Å ± 2Å	26Å ± 2Å
$2 \times 10^{15} cm^{-2}$	6Å ± 2Å	29Å ± 2Å
$5 \times 10^{15} cm^{-2}$	12Å ± 3Å	33Å ± 3Å

Table 4. Implantation Parameters

Parameter	Ni	Mo	Au
Implantation energy (keV)	3000	150	1000
Range, $\overline{X}$ (Å)	7450	295	1037
Straggle, $\overline{\Delta x}$ (Å)	1800	140	388
Estimated surface fraction	<0.001%		<0.1%
Deposited surface energy:			
electronic (eV/Å)	250	83	195
nuclear (eV/Å)	26	255	367
Integrated deposited surface energy: at $1 \times 10^{15} ions/cm^2$:			
electronic (eV/atom)	390	129	304
nuclear (eV/atom)	41	397	572

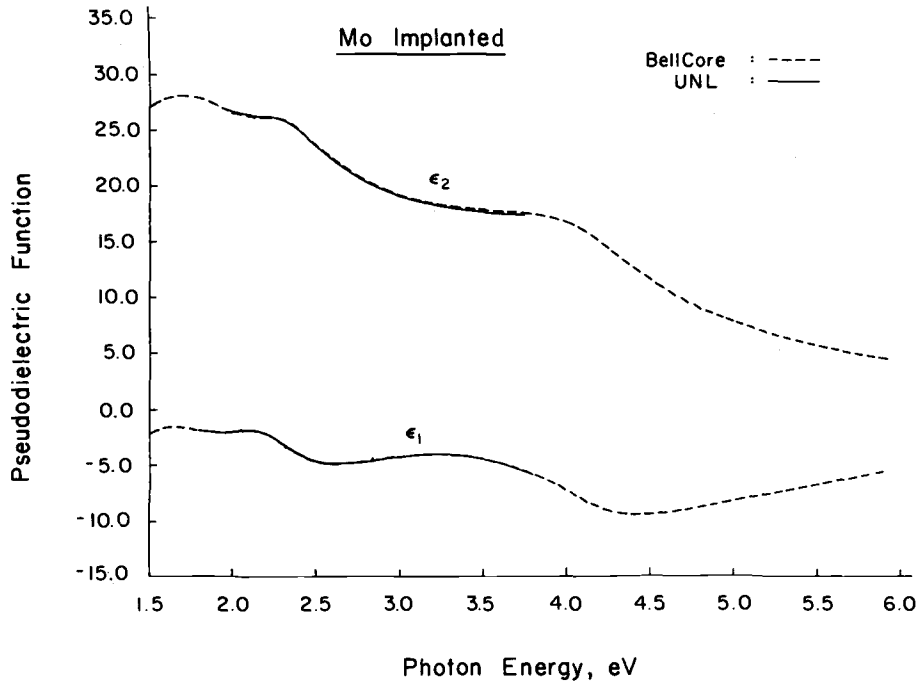

Figure 1. Pseudodielectric functions of the $5x10^{14} cm^{-2}$ fluence region of the Mo implanted mirror, measured by the two different ellipsometers used in this investigation, as described in the text.

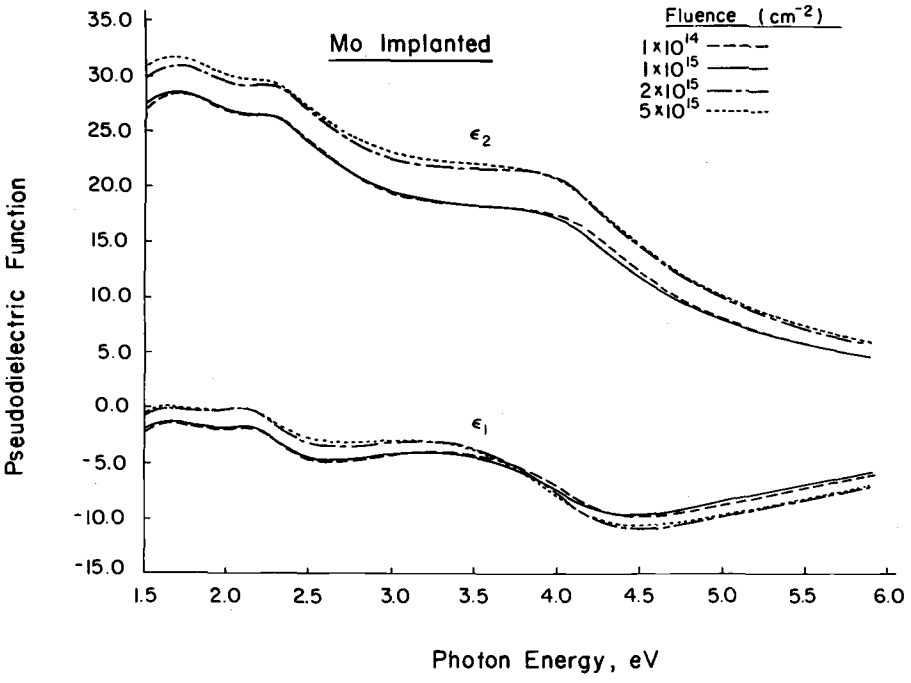

Figure 2. Pseudodielectric functions of the Mo implanted mirror as a function of fluence. (Bellcore ellipsometer)

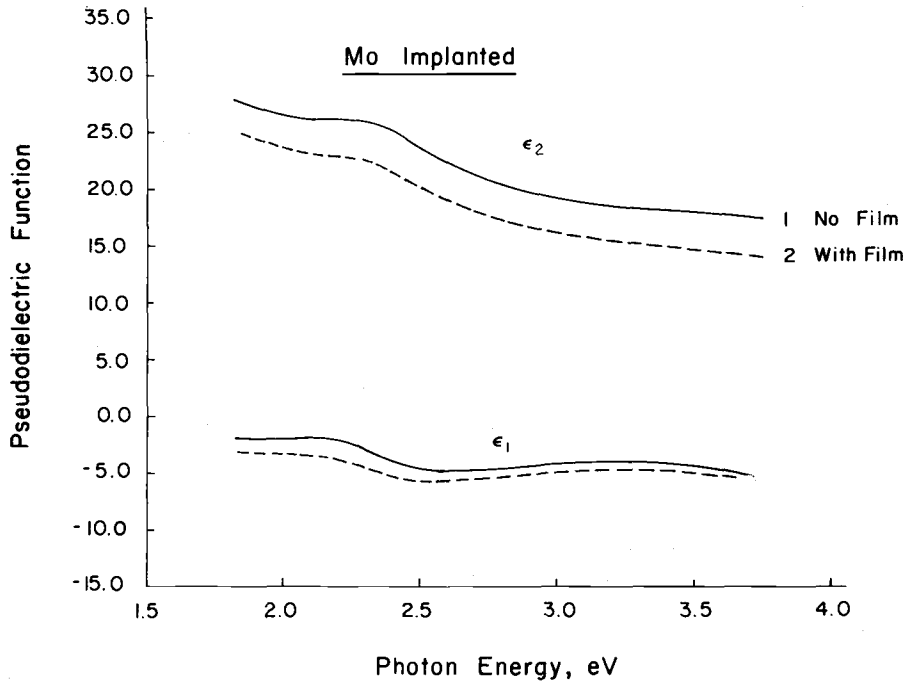

Figure 3. Pseudodielectric functions of an Mo surface after cleaning (solid lines), and of the same surface after several days in air (dashed lines).

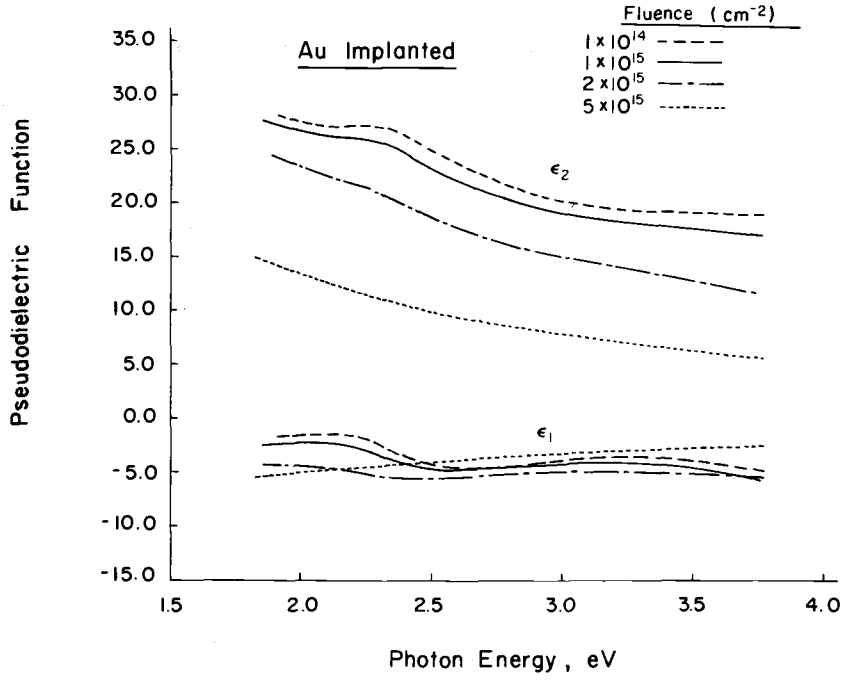

Figure 4. Pseudodielectric functions of the Au implanted mirror as a function of fluence. The 2×10^{14} cm^{-2} and 5×10^{14} cm^{-2} regions were almost identical to the 1×10^{14} cm^{-2} region (UNL ellipsometer).

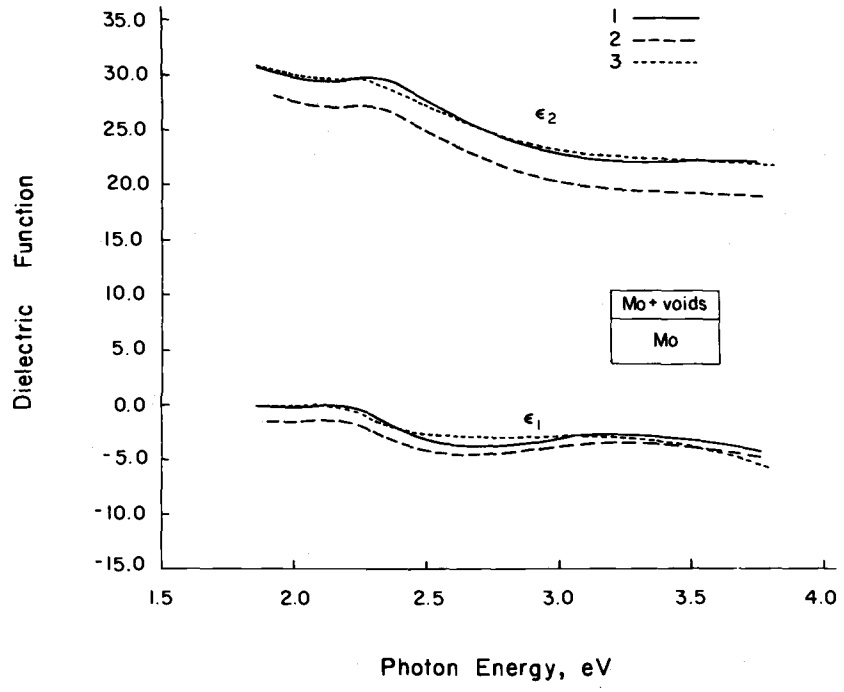

Figure 5. Dielectric function of the 1 x $10^{14}cm^{-2}$ fluence region of the Au-implanted mirror, calculated by correcting the data for 12A roughness (curve 1); pseudodielectric function data of the same region (curve 2); pseudodielectric function data of the 5 x $10^{15}cm^{-2}$ fluence region of the Mo-implanted mirror (curve 3). Inset: 3 phase model used to correct data for surface microscopic roughness.

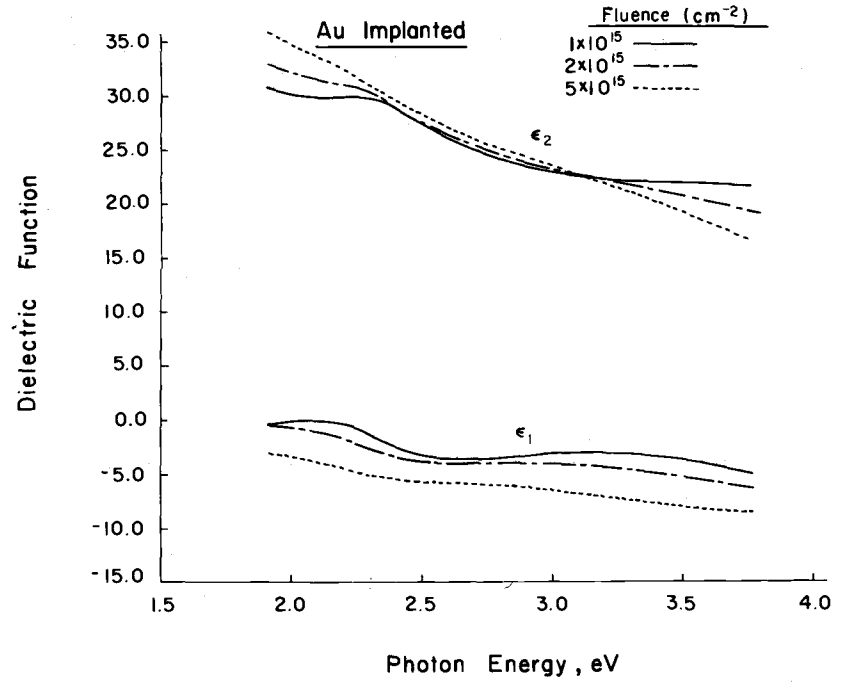

Figure 6. Dielectric functions of the Au implanted mirror, calculated by correcting the corresponding pseudodielectric function for microscopic roughness. The thicknesses and void fractions obtained from the calculations are given in Table II.

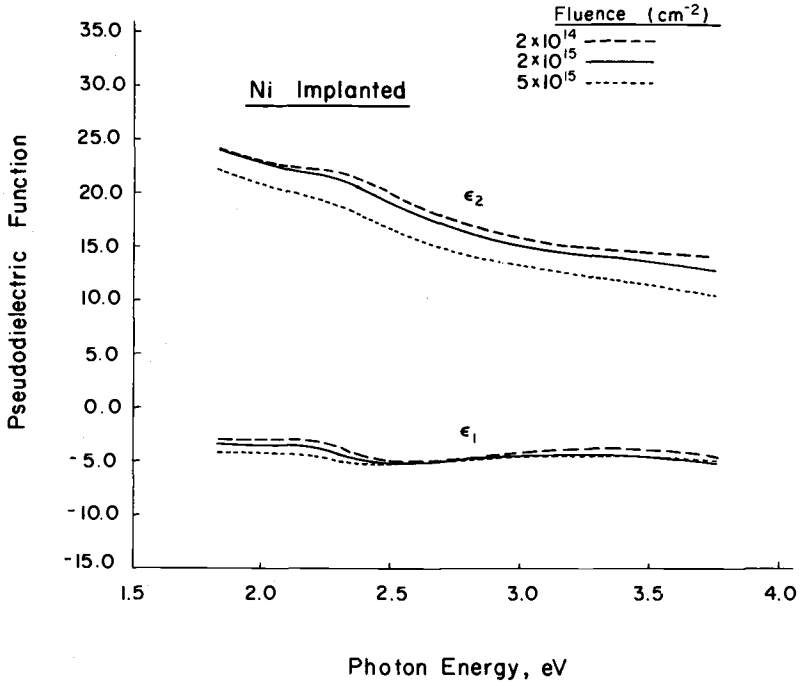

Figure 7. Pseudodielectric functions of the Ni implanted mirror, as a function of fluence (UNL ellipsometer).